Cumhuriyet Sci. J., 45(2) (2024) 386-393
DOI: https://doi.org/10.17776/csj.1420790

Cumhuriyet Science Journal

| csj.cumhuriyet.edu.tr | Founded: 2002 ISSN: 2587-2680 e-ISSN: 2587-246X Publisher: Sivas Cumhuriyet University

The Nonlinear Optical Properties of Self-Assembled InAs/GaAs Quantum Dot: Effect of Hydrostatic Pressure and Temperature

M. Jaouane [1,a], K. El-Bakkari [1,b], E. B. Al [2,c,*], A. Sali [1,d], F. Ungan[2,e]

[1] *Department of Physics, Laboratory of Solid-State Physics (LPS), Dhar El Mahraz Sidi Mohamed Ben Abdellah University, Fez 1796, Morocco.*

[2] *Department of Physics, Faculty of Science, Sivas Cumhuriyet University, 58140, Sivas, Türkiye.*

**Corresponding author*

Research Article

History
Received: 21/02/2024
Accepted: 02/05/2024

ABSTRACT

In this study, we have investigated the effects of temperature (T) and hydrostatic pressure (P) on both the nonlinear and linear optical properties of an InAs/GaAs core/shell quantum dot (QD) system with a Screened-Modified Kratzer potential (SMKP). To achieve this objective, we calculated the energy levels and their corresponding wave functions of the structure using the diagonalization method within the framework of the effective mass approximation. Analytical expressions for the absorption coefficients (ACs) and relative refractive index changes (RRICs) were derived using the compact-density-matrix approach. In our numerical calculations, we first determined the variation of the SMKP dependence, the dipole transition matrix element, and the electron energies of the ground (1s) and first excited state (1p) over a range of hydrostatic pressure (P) and temperature (T). As a result, the obtained numerical calculations revealed that changes in P and T influence both the magnitude and position of the resonant peaks that define the ACs and RRICs.

Keywords: Screened Modified Kratzer potential, Temperature, Hydrostatic pressure, Nonlinear optical properties.

[a] *mohammed.jaouane@gmail.com* *https://orcid.org/0000-0002-5779-8055*
[b] *elbakkari.kamal@gmail.com* *https://orcid.org/0000-0003-3649-7373*
[c] *emrebahadiral@hotmail.com* *https://orcid.org/0000-0003-4435-2879*
[d] *sali_ahm@hotmail.com* *https://orcid.org/0000-0003-4153-3404*
[e] *fungan@cumhuriyet.edu.tr* *https://orcid.org/0000-0003-3533-4150*

Introduction

Quantum confinement, observed in low-dimensional systems such as quantum wells [1,2], quantum wires [3], and quantum dots (QDs) [4], gives rise to novel properties. Particularly noteworthy are QDs, which possess naturally occurring atomic-like discrete energy levels. These physical attributes can be manipulated and fine-tuned by adjusting their size, composition, and even their shapes, which encompass a diverse range including approximations of spheres [5,6], rings [7], cubes [8,9], cylinders [10,11], pyramids [12], and ellipsoids [13]. QDs have captured the attention of numerous researchers in both experimental and theoretical [14] realms, rendering them valuable for an array of advanced optoelectronic and quantum devices. Such applications span from solar cells, lasers, batteries, and energy storage systems to light-emitting diodes, transistors, and beyond.

The QDs can be synthesized using a range of semiconductor materials. Within the realm of III-V semiconductors, indium arsenide (InAs) has garnered substantial significance and stands out as the most extensively utilized material for QD fabrication. In the form of a thin layer, InAs can be grown on GaAs substrates despite a notable lattice mismatch of approximately 6.8% [15]. The InAs/GaAs QD structure can be produced using various growth modes, including the Stranski-Krastanov (S-K) mode and the sub-monolayer (SML) mode, both referred to as self-assembled QDs [16]. The application of hydrostatic pressure and temperature to InAs/GaAs QDs renders them versatile materials, finding widespread utility in optical communications [17], laser technology [18], infrared detectors, and quantum-dot diodes [19].

Following the 1960 invention of the laser, nonlinear optics, a sub-discipline within modern optics, has found widespread applications. The behavior of materials in nonlinear optics can be characterized by macroscopic parameters, notably the refractive index and absorption coefficient, both of which are functions of the amplitude of the incident light's electric field [20]. In light of this, numerous scholars have directed their attention in recent years towards the study of these properties. For instance, Al et al. conducted an investigation into the nonlinear optical properties of a double GaAs/$Al_{1-x}Ga_xAs$ QW [21]. Ungan et al. [22] undertook simulations to examine the impact of electric and magnetic fields on nonlinear optical rectification, while Jaouane et al. [23] analyzed numerical outcomes concerning the nonlinear optical properties of multilayer cylindrical QDs. Jaouane et al. [24] conducted simulations to study the optical properties of allowed transitions, specifically the 1s-1p transition, within CdSe/ZnTe core/shell QDs using the screened modified Kratzer potential. Additionally, Edet et al. [25,26] explored the influence of magnetic fields and quantum confinement parameters on the optical properties of GaAs spherical QDs with the screened modified Kratzer potential in their papers. These properties have formed the fundamental basis for a variety of optoelectronic

devices, including far-infrared photodetectors, optical switches, far-infrared laser amplifiers, and optical modulators.

The purpose of this paper is to explore nonlinear optical properties by solving the Schrödinger equation, which describes electron states within quantum dots (QDs). This investigation is grounded in a modeling approach that employs the Screened Modified Kratzer potential (SMKP) to depict quantum confinement. In this context, we initially assessed how changes in temperature and hydrostatic pressure affect the energy eigenvalues and eigenfunctions of an InAs/GaAs core-shell quantum dot enclosed by the SMKP potential. This assessment was conducted using the diagonalization method within the framework of the effective mass approach. Subsequently, we utilized these energy eigenvalues and eigenfunctions to determine the absorption coefficients and refractive index changes of the system. The paper will be organized as follows: Section 2 will be dedicated to our theoretical model. In Section 3, we will present our numerical results along with their analysis, and a comprehensive summary will be provided in Section 4.

Theory

Schrödinger's wave equation

In this study, we considered a QD with SMKP. While $InAs$ forms the core of QD, the shell material is chosen as $GaAs$. We examined the system under pressure (P) and temperature (T) effects. Under these effects, within the framework of the effective mass approach, the Hamiltonian in spherical coordinates for the confined electron takes the form [26]

$$H = -\frac{\hbar^2}{2m^*(P,T)r^2}\left[\frac{\partial}{\partial r}\left(r^2\frac{\partial}{\partial r}\right) + \frac{1}{\sin\theta}\frac{\partial}{\partial\theta}\left(\sin\theta\frac{\partial}{\partial\theta}\right) + \frac{1}{\sin^2\theta}\frac{\partial^2}{\partial\phi^2}\right] + V(r,P,T), \quad (1)$$

where, $\hbar$ is the reduced Planck constant and $m^*(P,T)$ is the conduction band electron effective mass for the Γ valley, which is given by Vurgaftman formula depending on the hydrostatic pressure and temperature as [27,28]

$$(P,T) = \frac{m_0}{1+2\gamma+\left[\frac{E_P^\Gamma\left(E_g^\Gamma+\frac{2}{3}\Delta_{SO}\right)}{E_g^\Gamma\left(E_g^\Gamma+\Delta_{SO}\right)}\right]}, \quad (2)$$

where m_0 is the free electron mass, γ is the Kane parameter, E_P^Γ is the energy associated with the momentum matrix element at Γ, Δ_{SO} is the spin-orbit splitting, and E_g^Γ is the energy gap at Γ defined by the empirical Varshni expression depending on pressure and temperature as [28,29]

$$E_g^\Gamma(P,T) = E_g^\Gamma(0,0) - \frac{\alpha T^2}{\beta+T} + DP, \quad (3)$$

where, $E_g^\Gamma(0,0)$ is the energy gap at $P = 0\ kbar$ and $T = 0\ K$, where D is the pressure coefficient and α and β are the temperature coefficients. All parameters used in our calculations for InAs and GaAs are listed in Table 1.

Table 1. Parameters accepted in our simulations for GaAs and InAs.

Parameters	$InAs$	$GaAs$
$E_g^\Gamma(0,0)\ (meV)$	533	1519
$\alpha\ (meV/K)$	0.276	0.5405
$\beta\ (K)$	83	204
$D\ (meV/kbar)$	7.7	10.8
$\Delta_{SO}\ (meV)$	390	341
$E_P^\Gamma\ (meV)$	21500	28800
γ	-2.9	-1.94

$V(r,P,T)$ given in Eq. (1) is the spherically symmetrical SMKP and it is given as a function of hydrostatic pressure and temperature by [24,25,30],

$$V(r,P,T) = V_c(P,T)\left(q - \frac{r_e e^{-ar}}{r}\right)^2, \quad (4)$$

where, $V_c(P,T) = Q_c\left[E_g^\Gamma(GaAs) - E_g^\Gamma(InAs)\right]$, ($Q_c = 0.7$) is the dissociation energy between InAs and GaAs materials, r_e is the internuclear distance, a is the screening parameter, and q is the control parameter.

In the presence of pressure and temperature, the energy levels and their associated wave functions are obtained with the three-dimensional Schrödinger equation corresponding to the Hamiltonian in Eq. (1) within the framework of the envelope function approach:

$$H\psi_{nlm}(r,\theta,\phi) = E_{nlm}\psi_{nlm}(r,\theta,\phi), \quad (5)$$

where, n, l, and m are the principal, angular and magnetic momentum quantum numbers, respectively. This three-dimensional Schrödinger equation of the system under consideration cannot be solved analytically under the effects of pressure and temperature. Therefore, we have to use the diagonalization method to calculate direct numerical solutions such as energy eigenvalues and envelope wave functions. Thus, the solutions of Eq. (5) can be obtained by the approach based on the extension of electronic states on a complete orthogonal basis in the form

$$\psi_{nlm}(r,\theta,\phi) = \sum_{j=1} c_{n_j}\psi^{(0)}_{n_jlm}(r,\theta,\phi) \quad (6)$$

where, c_n is the expansion coefficient and the electronic states are categorized according to certain l and m values. $\psi^{(0)}_{nlm}(r,\theta,\phi)$ is the total wave function describing the motion of the electron and the exact solution for an electron in a spherical QD with infinite potential is given by

$$\psi^{(0)}_{nlm}(r,\theta,\phi) = \varphi^{(0)}_{nl}(r)Y_{lm}(\theta,\phi), \quad (7)$$

here, $\varphi_{nl}^{(0)}(r)$ is the radial part of the electron eigenfunction and it is given by

$$\varphi_{nl}^{(0)}(r) = \begin{cases} Nj_l(k_n r), & r < r_I \\ 0, & r \geq r_I, \end{cases} \quad (8)$$

where N is the normalization constant, k_n is the nth root of the lth order spherical Bessel function-j_l, and $r_I = 20\ nm$ is the radius of the infinite spherical QD. $Y_{lm}(\theta, \phi)$ in Eq. (7) are spherical harmonics.

Optical properties

After obtaining the energies and their associated envelope wave functions, the effects of pressure and temperature on the ACs and RRICs can be calculated using the density matrix approach. In this study, we use electromagnetic radiation polarized in the z direction. This electromagnetic radiation is considered as

$$E(t) = E_0 \cos \omega t = \bar{E} e^{i\omega t} + \bar{E}^* e^{-i\omega t}, \quad (9)$$

where $\bar{E}$ and ω are the amplitude and angular frequency of the electric field, respectively.

In the two-level system approach, the linear and third-order nonlinear ACs are given respectively by [24]

$$\alpha^{(1)}(\omega) = \sqrt{\frac{\mu}{\varepsilon_r}} \frac{\sigma_s |M_{12}|^2 \hbar\omega \Gamma_{12}}{(E_{12} - \hbar\omega)^2 + (\hbar\Gamma_{12})^2} \quad (10)$$

and

$$\alpha^{(3)}(\omega, I) = -\sqrt{\frac{\mu}{\varepsilon_r}} \frac{2I}{n_r \varepsilon_0 c} \frac{\sigma_s |M_{12}|^4 \hbar\omega \Gamma_{12}}{[(E_{12} - \hbar\omega)^2 + (\hbar\Gamma_{12})^2]^2} \left[1 - \frac{\delta_{12}^2}{4|M_{12}|^2} \frac{3E_{12}^2 - 4E_{12}\hbar\omega + \hbar^2(\omega^2 - \Gamma_{12}^2)}{E_{12}^2 + (\hbar\Gamma_{12})^2}\right], \quad (11)$$

where, $\mu = 4\pi \times 10^{-7}\ H/m$ is the magnetic permeability of the vacuum, $\varepsilon_r = \sqrt{\varepsilon_r(InAs)\varepsilon_r(GaAs)}$ is the average dielectric constant of the QD material, σ_s is the volume density of the carriers in the system, $I = 2\varepsilon_0 n_r c |\bar{E}|^2$ represents the incident optical intensity, $n_r = \sqrt{\varepsilon_r}$ is the refractive index, $\varepsilon_0 = 8.854 \times 10^{-12}\ F/m$ is the dielectric constant of vacuum, c is the speed of light in vacuum, $\delta_{12} = |M_{11} - M_{22}|$ is the mean electron displacement, $M_{12} = \langle \psi_1 | er | \psi_2 \rangle$ are the off-diagonal matrix elements of the electric dipole moment, $E_{12} = E_2 - E_1$ is the intraband transition energy between the first excited state and the ground state, $\hbar\omega$ is the incident photon energy, $\Gamma_{12} = 1/T_{12}$ is the relaxation ratio between the ground and excited state and T_{12} is the damping term associated with the lifetime of the electron involved in the transitions.

The total AC is given as

$$\alpha(\omega, I) = \alpha^{(1)}(\omega) + \alpha^{(3)}(\omega, I) \quad (12)$$

By the same approach, linear, third-order nonlinear and total RRICs are given respectively with [31]

$$\frac{\Delta n^{(1)}(\omega)}{n_r} = \frac{1}{2n_r^2 \varepsilon_0} \frac{\sigma_s (E_{12} - \hbar\omega) |M_{12}|^2}{(E_{12} - \hbar\omega)^2 + (\hbar\Gamma_{12})^2}, \quad (13)$$

$$\frac{\Delta n^{(3)}(\omega, I)}{n_r} = -\frac{\mu c I \sigma_s |M_{12}|^4}{n_r^3 \varepsilon_0} \frac{E_{12} - \hbar\omega}{[(E_{12} - \hbar\omega)^2 + (\hbar\Gamma_{12})^2]^2} \left[1 - \frac{\delta_{12}^2 \left[E_{12}^2 - E_{12}\left(\hbar\omega + \frac{(\hbar\Gamma_{12})^2}{E_{12} - \hbar\omega}\right) - 2(\hbar\Gamma_{12})^2\right]}{4|M_{12}|^2 [E_{12}^2 + (\hbar\Gamma_{12})^2]}\right] \quad (13)$$

and

$$\frac{\Delta n(\omega, I)}{n_r} = \frac{\Delta n^{(1)}(\omega)}{n_r} + \frac{\Delta n^{(3)}(\omega, I)}{n_r}, \quad (14)$$

The intraband optical transition probability amplitude between two electronic states, such as lowest and first excited, is proportional to the matrix element of the electric dipole moment. Except for the selection rules $\Delta l = \pm 1$ and $\Delta m = 0, \pm 1$, the matrix elements of the electric dipole moment become 0. Therefore, in this study, we consider the transition between the $1s$ ($l = 0, m = 0$) and $1p$ ($l = 1, m = 0$) electron states.

Results and discussions

The aim of this study is to adjust and optimize the ACs and RRICs in a QD system with SMKP under the effects of applied pressure and temperature. The parameters adopted in our calculations are as follows: $r_e = 0.5$, $a = 0.05$, $q = 1.1$, $\varepsilon_r(InAs) = 15.15$, $\varepsilon_r(GaAs) = 12.88$, $T_{12} = 0.5\ ps$, $\sigma = 3 \times 10^{22}\ m^{-3}$ and $I = 50\ MW/m^2$.

In this section, we explore the influences of temperature and pressure on the linear and nonlinear optical properties of core/shell QDs with SMKP. Firstly, we have plotted the shape of the SMKP given by Eq. (4) and the electron probability density of the first two states ($1s$ and $1p$) against the distance r for different values of P, where the temperature is set to be $T = 0\ K$ in Figure 1a and for different values of T at $P = 0\ kbar$ in Figure 1b. This figure clearly shows that the $V(r)$ has a local minimum at a critical distance r_c. This minimum value shifts to the left side (lower values of r) with an increment of the hydrostatic pressure (Figure 1a). It caused by the shrinkage of the QD size under the pressure. Whereas the r_c moves to the right side (higher values of r) with the increase of the temperature (Figure 1b), resulting from the extension of interatomic distance due to rising of temperature. In addition, it can be confirmed that the effects of P and T on the $V(r, P, T)$ are not significant for smaller values of the r, due to the strong confinement effect in these regions. Additionally, it can be seen that an enhance in the hydrostatic pressure causes an increase in the well depth, while an increase in the temperature causes a decrease, and therefore, the area localization of the electron is increased (decreased) with the increase of the hydrostatic pressure (temperature), which is totally agree with the results of the electron probability density reported in the same figure. These results show clearly that the influences of the temperature and pressure have a significant impact in the nonlinear and linear optical properties in the core/shell QDs with SMKP.

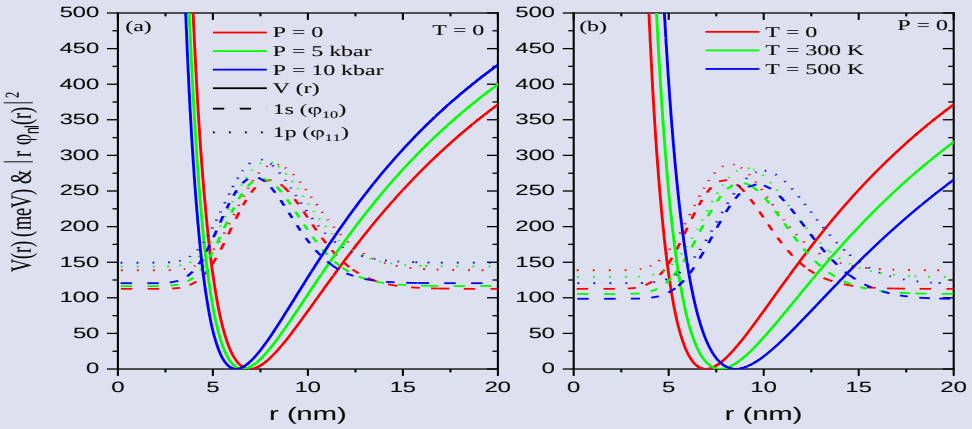

Figure 1. Profiles of SMKP (solid line) and the electron probability density of the first two states $1s$ (dashed line) and $1p$ (pointed line) as a function of r for different values of P $(0, 5\ and\ 10\ kbar)$ at $T = 0K$ (a), and for different values of T $(0, 300$ and $500\ K)$ at $P = 0\ kbar$ (b).

To understand how the energy eigenvalues of electrons change with temperature and pressure, we have plotted Figure 2 the electron energies of the ground 1s and first excited state 1p versus temperature for different values of P. It is clearly seen that the values of the first excited state are higher than those of the ground one, due to the feeble confinement of the electron wave function in the latter, which is confirmed in the results in Figure 1 related to the electron density probability. Furthermore, we can notice that for a fixed value of the T, the rise in hydrostatic pressure increases the energy eigenvalues. This result is due to the augmentation of the electron effective mass and the height of the SMKP with the pressure. On the other hand, for a given value of applied P, the electron energies of the first two states decreases with an increase in the T. This behavior can be explained as follows: An increase in temperature leads to an extension of the interatomic distance, which in turn diminishes the gap energy, thereby reducing quantum confinement [23]. Moreover, as the temperature takes high values, the Bohr radius is increased due to the reducing effective mass. In addition, the contribution of the temperature increases the thermal agitation in the system which can increase the energy of the electron. Therefore, the value of the Rydberg constant decreases, which in turn diminishes the height of the barrier potential. As a consequence, the electron becomes less confined, and the energy eigenvalues decreases with the T.

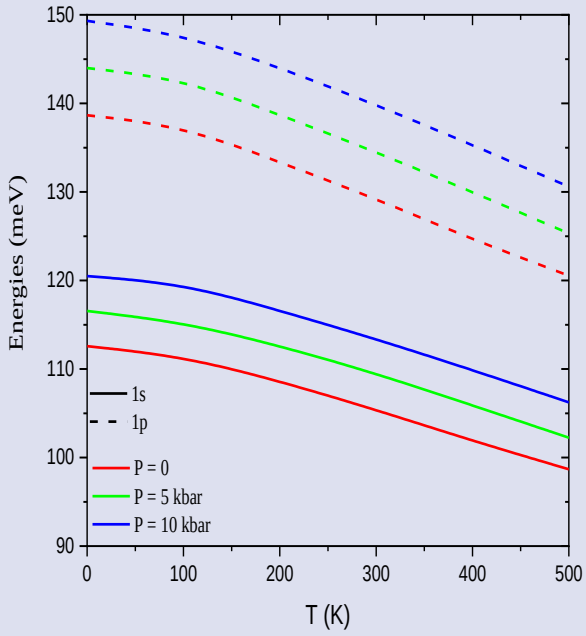

Figure 2. Electron energies of the ground state $1s$ (solid line) and first excited state $1p$ (dashed line) versus the temperature for different values of P $(0, 5\ and\ 10\ kbar)$.

Before presenting our numerical results of the ACs and RRICs in a QD system with SMKP, it is useful to make a study of the changes in the difference energy E_{12} as well as in the electric dipole moment matrix element M_{12}. For this reason, the variation in the E_{12} and M_{12} versus the temperature for three different values of P have been plotted in Figure 3a and Figure 3b respectively. It can be observed that for a given value of T, the transition energy increases when the pressure is enhanced. A comparable behavior was noticed in δ–doped quantum well in $GaAs$ [32]. This is because that the hydrostatic pressure creates

an additional confinement, which makes the electron more confined in the dot and the E_{12} increases with P.

While the opposite occurs in the case of temperature, as it increases, the extension between the energy levels reduces due to diminishing of quantum confinement, making energy transitions less important. This outcome has also been reported Ref. [33].

Furthermore, the observation in Figure 3b shows that for a fixed value of P, the increase of temperature enhances the dipole moment matrix element, which is proportional to the overlap of the electron wavefunctions, the ground and excited states (see Figure 1) consequently, the M_{12} is increased with increasing the temperature. In addition, for a fixed value of T, if the hydrostatic pressure rises, the reverse happens and the M_{12} decreases. This kind of outcome has also been described in different geometries by some authors [34–36]. The reduction in the dipole matrix element with respect to pressure (P) can be explained by the decrease in the area where the electron is localized in our system. This is mainly due to the increase in the depth of the SMKP, as demonstrated in Figure 1b.

To explore the dependence of the optical properties on the external perturbations (P and T) in a QD system with SMKP, we have drawn in Figure 4 the calculation results of the nonlinear (dotted), linear (dashed) and total (solid) ACs for the $1s \rightarrow 1p$ allowed transition, versus the incident photon energy $\hbar\omega$ for various values of pressure at $T = 0\,K$ (Figure 4a) and for different values of temperature at $P = 0$ kbar (Figure 4b). We can note from Eqs. (10) and (11) that the E_{12} and M_{12} are two significant parameters in the determining of ACs. Indeed, the ACs has a maximum value when the incoming photon energy $\hbar\omega$ coincides with the transition energy E_{12}, which is referred as the resonance photon energy and the amplitudes of ACs peaks are proportional to M_{12}. Furthermore, it can be clearly seen from this figure that the hydrostatic pressure P induces a blueshift of the peak of the ACs. These outcomes can be explained in the following way: The application of hydrostatic pressure reinforces the quantum confinement of the electron in the QD and leads to stretching the quantized energy levels hence the growth the energy transition. This is in good agreement with the findings obtained in Figure 3 and also those of Ref. [35].

Additionally, the value of the ACs reduces as the pressure rises from 0 to 10 $kbar$. The physical reason of this result is that as the P goes up, the electron wave functions are extremely confined inside the QD. This outcome is in agreement with Ref. [34]. However, in contrast to the P effect, the amplitude of the resonant peaks of the ACs increases with increasing T from 0 to $500\,K$ as shown in Figure 4b. The reason for this behavior is that the value of the M_{12} increases with T (see Figure 3b). Another finding is that the position of the resonant peaks displays a shift toward the lower incident photon energy as the T increases. This redshift comes from diminishing the confinement potential and effective mass of the electron with growing of the temperature. All these descriptions can be understood by observing the variation of the numerical values of M_{12} and E_{12} with the P and T in the Figure 3.

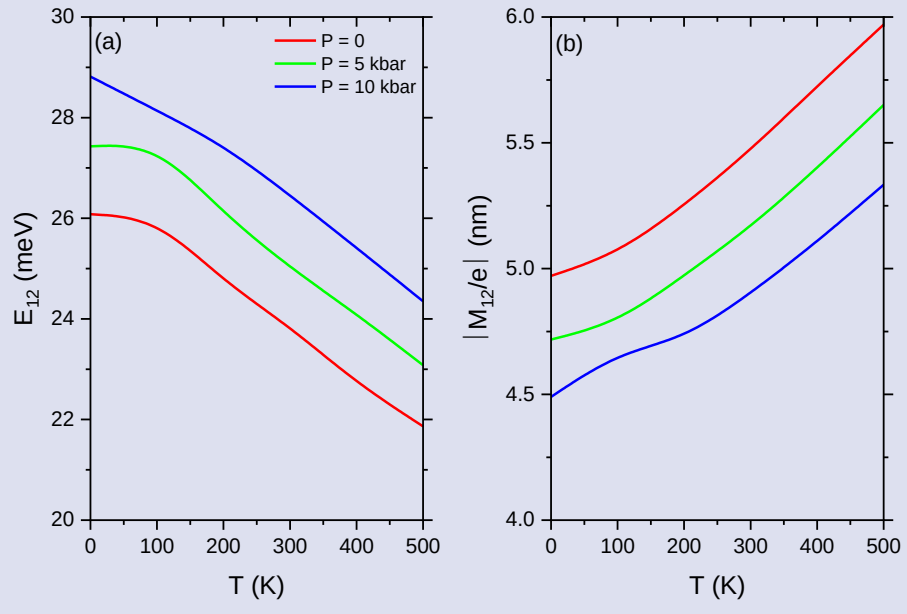

Figure 3. Shows (a) the intraband transition energy between the $1p$ state and the $1s$ state versus temperature, and (b) the matrix elements of the electric dipole moment as a function of T, for different values of P.

In order to investigate the influence of variations of the P and T on the relative refractive index changes, we have computed in Figure 5 the variation of the nonlinear (dotted), linear (dashed) and total (solid) RRICs for the $1s \rightarrow 1p$ against the incident photon energy $\hbar\omega$. The exploited parameters are similar as in the previous Figure

4. This figure clearly displays that the RRICs are related to the hydrostatic pressure and temperature. By increasing the pressure (temperature), maxima and minima of the RRICs decrease (increase) and the peak position shifts toward higher (lower) energies. This is because the transition energy difference E_{12} increases (decreases) when the P (T) rises. Because the physical parameters such as electron effective mass and barrier height increases (decrease) with the P (T). These numerical results are well-matched with the variation of ACs under the effects of P and T in Figure 4. These characteristics make QDs very promising candidates for nonlinear optical materials.

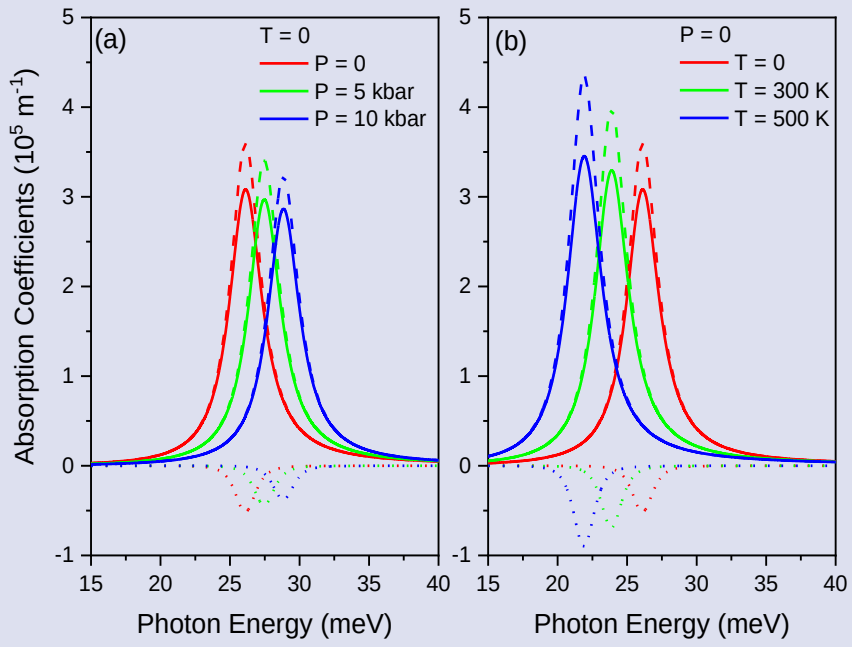

Figure 4. Plot of nonlinear, linear, and total ACs for allowed optical transition 1s→1p against the photon energy for three diverse values of pressures (a) and temperatures (b).

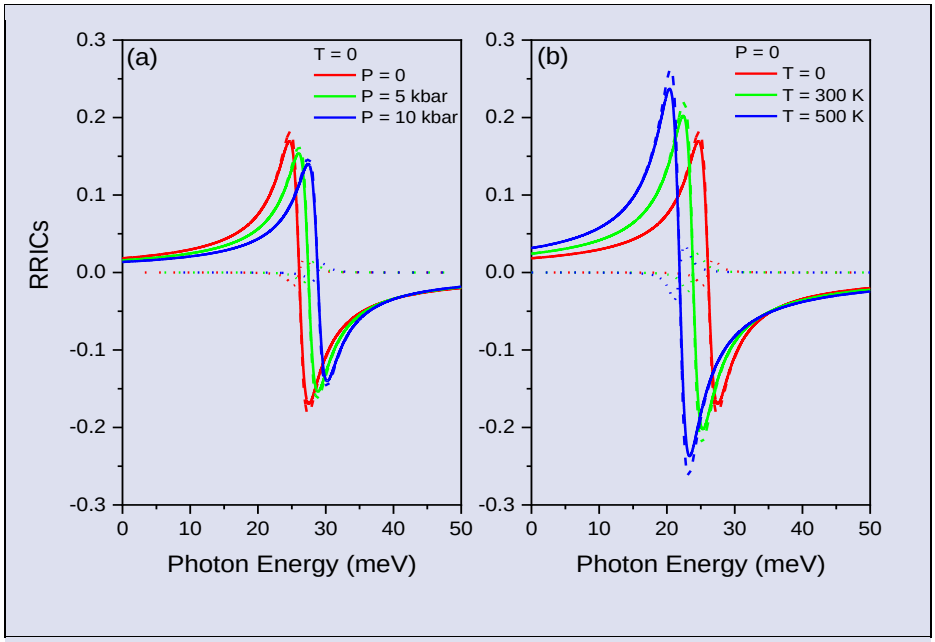

Figure 5. Plot of nonlinear, linear, and total RRICs for the $1s \rightarrow 1p$ transition against the photon energy for three diverse values of pressures (a) and temperatures (b).

Conclusion

In this work, a numerical calculation has been performed to examine the effects of temperature and pressure on the electron probability density of $1s$ and the $1p$ states, transition energy of the electron, dipole moment matrix element, nonlinear and linear ACs and RRICs of a $InAs/GaAs$ core/shell QD system. The electronic quantum confinement is modeled by the SMKP. To derive the wave functions and their associated energy levels, the Schrödinger equation was resolved by diagonalization method. Numerical outcomes reveal that the depth of SMKP, E_{12}, M_{12}, ACs and RRICs of our system are strongly influenced by the variation of the temperature and pressure. It was obtained that the ACs and RRICs are related to the pressure and temperature. As the pressure (temperature) increases, the resonance peaks of ACs and RRICs decrease (increase) and also shift towards higher (lower) energies. It has also been exposed that the effects of P and T on the depth of SMKP are significant in large distance r of QD.

Acknowledgments

M. Jaouane, K. El-Bakkari and A. Sali wrote the “Abstract”, “Introduction”, “Results and discussion”, and “Conclusion” sections of the article.

E. B. Al wrote the program, got the results, drew the graphs, wrote the “Theory” section and edited the article.

F. Ungan determined the problem and the title and edited the article.

Conflicts of interest

There are no conflicts of interest in this work.

Data Availability Statement

Data will be made available on reasonable request.

References

[1] Yesilgul U., Ungan F., Sakiroglu S., Sari H., Kasapoglu E., Sökmen I., Nonlinear optical properties of a semi-exponential quantum wells: Effect of high-frequency intense laser field, *Optik (Stuttg).,* 185 (2019) 311–316.

[2] Belaid W., El Ghazi H., Zaki S.E., Basyooni M.A., Tihtih M., Ennadir R., Kılıç H.Ş., Zorkani I., Jorio A., A theoretical study of the effects of electric field, hydrostatic pressure, and temperature on photoionization cross-section of a donor impurity in (Al, Ga)N/AlN double triangular quantum wells, *Phys. Scr.,* 98 (2023) 045913.

[3] Sali A., Fliyou M., Satori H., Loumrhari H., Photoionization of Impurities in Quantum-Well Wires, *Phys. Status Solidi.,* 211 (1999) 661–670.

[4] Sali A., Satori H., The combined effect of pressure and temperature on the impurity binding energy in a cubic quantum dot using the FEM simulation, *Superlattices Microstruct.,* 69 (2014) 38–52.

[5] Fakkahi A., Sali A., Jaouane M., Arraoui R., Hydrostatic pressure, temperature, and electric field effects on the hydrogenic impurity binding energy in a multilayered spherical quantum dot, *Appl. Phys. A.,* 127 (2021) 908.

[6] Fakkahi A., Sali A., Jaouane M., Arraoui R., A. Ed-Dahmouny, Study of photoionization cross section and binding energy of shallow donor impurity in multilayered spherical quantum dot, *Physica E*., 143 (2022) 115351.

[7] El-Bakkari K., Sali A., Iqraoun E., Ezzarfi A., Polaron and conduction band non-parabolicity effects on the binding energy, diamagnetic susceptibility and polarizability of an impurity in quantum rings, *Superlattices Microstruct.,* 148 (2020) 106729.

[8] Arraoui R., Sali A., Ed-Dahmouny A., Jaouane M., Fakkahi A., Polaronic mass and non-parabolicity effects on the photoionization cross section of an impurity in a double quantum dot, *Superlattices Microstruct*., 159 (2021) 107049.

[9] Ed-Dahmouny A., Sali A., Es-Sbai N., Arraoui R., Jaouane M., Fakkahi A., El-Bakkari K., Duque C.A., Combined effects of hydrostatic pressure and electric field on the donor binding energy, polarizability, and photoionization cross-section in double GaAs/Ga 1-x Al x As quantum dots, *Eur. Phys. J. B*., 95 (2022).

[10] Jaouane M., Sali A., Kasapoglu E., Ungan F., Tuning of nonlinear optical characteristics of a cylindrical quantum dot by external fields and structure parameters, *Philos. Mag*., (2023) 1–19.

[11] Jaouane M., Sali A., A. Ezzarfi A., A. Fakkahi A., Arraoui R., Study of hydrostatic pressure, electric and magnetic fields effects on the donor binding energy in multilayer cylindrical quantum dots, *Physica E*., 127 (2021) 114543.

[12] Jaouane M., Fakkahi A., Ed-Dahmouny A., El-Bakkari K., Tuzemen A.T., Arraoui R., Sali A., Ungan F., Modeling and simulation of the influence of quantum dots density on solar cell properties, *Eur. Phys. J. Plus*., 138 (2023) 148.

[13] Ed-Dahmouny A., Zeiri N., Fakkahi A., Arraoui R., Jaouane M., Sali A., Es-Sbai N., El-Bakkari K., Duque C.A., Impurity photo-ionization cross section and stark shift of ground and two low-lying excited electron-states in a core/shell ellipsoidal quantum dot, *Chem. Phys. Lett*., 812 (2023) 140251.

[14] Tiutiunnyk A., Tulupenko V., Mora-Ramos M.E., Kasapoglu E., Ungan F., Sari H., Sökmen I., Duque C.A., Electron-related optical responses in triangular quantum dots, *Physica E*., 60 (2014) 127–132.

[15] Li G.H., Goñi A.R., Abraham C., Syassen K., Santos P.V., Cantarero A., Brandt O., Ploog K., Photoluminescence from strained InAs monolayers in GaAs under pressure, *Phys. Rev. B*., 50 (1994) 1575–1581.

[16] Du Park G., Du Ha J., Kang T.I., Kim J.S., Kim Y., Lee S.J., Han I.S., Investigation of junction electric fields for InAs quantum dot solar cells with photoreflectance spectroscopy, *Curr. Appl. Phys*., 50 (2023) 46–52.

[17] Zhou P.Y., Dou X.M., Wu X.F., Ding K., Li M.F., Ni H.Q., Niu Z.C., Jiang D.S., Sun B.Q., Single-photon property characterization of 1.3 μm emissions from InAs/GaAs quantum dots using silicon avalanche photodiodes, *Sci. Rep*., 4 (2014) 3633.

[18] Bimberg D., Ledentsov N.N., Grundmann M., Kirstaedter N., Schmidt O.G., Mao M.H., Ustinov V.M., Egorov A.Y., Zhukov A.E., Kopév P.S., Alferov Z.I., Ruvimov S.S., Gösele U., Heydenreich J., InAs-GaAs quantum pyramid lasers: In situ growth, radiative lifetimes and polarization properties, *Japanese J. Appl. Physics*., 35 (1996) 1311–1319.

[19] Wang T., Lee A., Tutu F., Seeds A., Liu H., Jiang Q., Groom K., Hogg R., The effect of growth temperature of GaAs nucleation layer on InAs/GaAs quantum dots monolithically grown on Ge substrates, *Appl. Phys*. Lett., 100 (2012) 052113.

[20] Li C., Nonlinear Optics, Springer Singapore, Singapore, 2017.

[21] Al E.B., Ungan F., Yesilgul U., Kasapoglu E., Sari H., Sökmen I., Effects of applied electric and magnetic fields on the nonlinear optical properties of asymmetric GaAs/Ga1-xAlxAs double inverse parabolic quantum well, *Opt. Mater.,* 47 (2015) 1–6.

[22] Ungan F., Martínez-Orozco J.C., Restrepo R.L., Mora-Ramos M.E., Kasapoglu E., Duque C.A., Nonlinear optical rectification and second-harmonic generation in a semi-parabolic quantum well under intense laser field: Effects of electric and magnetic fields, *Superlattices Microstruct.,* 81 (2015) 26–33.

[23] Jaouane M., Sali A., Fakkahi A., Arraoui R., Ungan F., The effects of temperature and pressure on the optical properties of a donor impurity in (In,Ga)N/GaN multilayer cylindrical quantum dots, *Micro and Nanostructures*, 163 (2022) 107146.

[24] Jaouane M., El-Bakkari K., Al E.B., Sali A., Ungan F., Linear and nonlinear optical properties of CdSe/ZnTe core/shell nanostructures with screened modified Kratzer potential, *Eur. Phys. J. Plus*., 138 (2023) 319.

[25] Edet C.O., Al E.B., Ungan F., Ali N., Ramli M.M., Asjad M., Effects of the confinement potential parameters and optical intensity on the linear and nonlinear optical properties of spherical quantum dots, *Results Phys*., 44 (2023) 106182.

[26] Edet C.O., Al E.B., Ungan F., Ali N., Rusli N., Aljunid S.A., Endut R., Asjad M., Effects of Applied Magnetic Field on the Optical Properties and Binding Energies Spherical GaAs Quantum Dot with Donor Impurity, *Nanomaterials*., 12 (2022) 2741.

[27] Makhlouf D., Choubani M., Saidi F., Maaref H., Applied electric and magnetic fields effects on the nonlinear optical rectification and the carrier's transition lifetime in InAs/GaAs core/shell quantum dot, *Mater. Chem. Phys*., 267 (2021) 124660.

[28] Makhlouf D., Choubani M., Saidi F., Maaref H., Modeling of the second harmonic generation in a lens-shaped InAs/GaAs quantum core/shell dot under temperature, pressure and applied electric field effects, *Results Phys*., 16 (2020) 102961.

[29] Makhlouf D., Choubani M., Saidi F., Maaref H., Applied electric and magnetic fields effects on the nonlinear optical rectification and the carrier's transition lifetime in InAs/GaAs core/shell quantum dot, *Mater. Chem. Phys*., 267 (2021) 124660.

[30] Edet C.O., Al E.B., Ungan F., Ali N., Rusli N., Aljunid S.A., Endut R., Asjad M., Effects of Applied Magnetic Field on the Optical Properties and Binding Energies Spherical GaAs Quantum Dot with Donor Impurity, *Nanomaterials*., 12 (2022) 2741.

[31] Al E.B., Peter A.J., Mora-Ramos M.E., Ungan F., Theoretical investigation of nonlinear optical properties of Mathieu quantum well, *Eur. Phys. J. Plus*, 138 (2023) 49.

[32] Oubram O., Rodríguez-Vargas I., Martínez-Orozco J.C., Refractive index changes in n-type delta-doped GaAs under hydrostatic pressure, *Rev. Mex. Fis*., 60 (2014) 161–167.

[33] Liang S., Xie W., Effects of the hydrostatic pressure and temperature on optical properties of a hydrogenic impurity in the disc-shaped quantum dot, *Physica B*., 406 (2011) 2224–2230.

[34] Farkoush B.A, Safarpour G., Zamani A., Linear and nonlinear optical absorption coefficients and refractive index changes of a spherical quantum dot placed at the center of a cylindrical nano-wire: Effects of hydrostatic pressure and temperature, *Superlattices Microstruct*., 59 (2013) 66–76.

[35] Rezaei G., Kish S.S., Linear and nonlinear optical properties of a hydrogenic impurity confined in a two-dimensional quantum dot: Effects of hydrostatic pressure, external electric and magnetic fields, *Superlattices Microstruct.,* 53 (2013) 99–112.

[36] Zhang Z.H., Yuan J.H., Guo K.X., The combined influence of hydrostatic pressure and temperature on nonlinear optical properties of GaAs/Ga0.7Al0.3As morse quantum well in the presence of an applied magnetic field, *Materials*., 11 (2018) 668.